

PPPL-5263

Preliminary measurements of the edge magnetic field pitch from 2-D Doppler backscattering in MAST and NSTX-U

R. G. L. Vann, K. J. Brunner, R. Ellis, G. Taylor, D. A. Thomas

September 2016



Prepared for the U.S. Department of Energy under Contract DE-AC02-09CH11466.

Princeton Plasma Physics Laboratory

Report Disclaimers

Full Legal Disclaimer

This report was prepared as an account of work sponsored by an agency of the United States Government. Neither the United States Government nor any agency thereof, nor any of their employees, nor any of their contractors, subcontractors or their employees, makes any warranty, express or implied, or assumes any legal liability or responsibility for the accuracy, completeness, or any third party's use or the results of such use of any information, apparatus, product, or process disclosed, or represents that its use would not infringe privately owned rights. Reference herein to any specific commercial product, process, or service by trade name, trademark, manufacturer, or otherwise, does not necessarily constitute or imply its endorsement, recommendation, or favoring by the United States Government or any agency thereof or its contractors or subcontractors. The views and opinions of authors expressed herein do not necessarily state or reflect those of the United States Government or any agency thereof.

Trademark Disclaimer

Reference herein to any specific commercial product, process, or service by trade name, trademark, manufacturer, or otherwise, does not necessarily constitute or imply its endorsement, recommendation, or favoring by the United States Government or any agency thereof or its contractors or subcontractors.

PPPL Report Availability

Princeton Plasma Physics Laboratory:

<http://www.pppl.gov/techreports.cfm>

Office of Scientific and Technical Information (OSTI):

<http://www.osti.gov/scitech/>

Related Links:

[U.S. Department of Energy](#)

[U.S. Department of Energy Office of Science](#)

[U.S. Department of Energy Office of Fusion Energy Sciences](#)

Preliminary measurements of the edge magnetic field pitch from 2-D Doppler backscattering in MAST and NSTX-U

R. G. L. Vann,¹ K. J. Brunner,² R. Ellis,³ G. Taylor,³ and D. A. Thomas^{1,4}

¹York Plasma Institute, Department of Physics, University of York, York YO10 5DD, UK

²Centre for Advanced Instrumentation, Department of Physics, Durham University, Durham DH1 3LE, UK

³Princeton Plasma Physics Laboratory, Princeton, New Jersey 08543, USA

⁴Culham Centre for Fusion Energy, Culham Science Centre, Abingdon OX14 3DB, UK

(Dated: 23 June 2016)

The Synthetic Aperture Microwave Imaging (SAMI) system is a novel diagnostic consisting of an array of 8 independently-phased antennas. At any one time, SAMI operates at one of 16 frequencies in the range 10-34.5GHz. The imaging beam is steered in software post-shot to create a picture of the entire emission surface. In SAMI's active probing mode of operation, the plasma edge is illuminated with a monochromatic source and SAMI reconstructs an image of the Doppler back-scattered (DBS) signal. By assuming that density fluctuations are extended along magnetic field lines, and knowing that the strongest back-scattered signals are directed perpendicular to the density fluctuations, SAMI's 2-D DBS imaging capability can be used to measure the pitch of the edge magnetic field. In this paper we present preliminary pitch angle measurements obtained by SAMI on the Mega-Amp Spherical Tokamak (MAST) at Culham Centre for Fusion Energy and on the National Spherical Torus Experiment Upgrade at Princeton Plasma Physics Laboratory. The results demonstrate encouraging agreement between SAMI and other independent measurements.

I. MOTIVATION

The stability and performance of tokamaks operating in the so-called high confinement mode ("H-mode") depends strongly on the transport barrier that develops in the plasma edge. The very narrowness of this layer (typically only $\sim 2\%$ of the minor radius) makes it difficult to characterise. An issue associated with H-mode operation is the appearance of edge localised modes (ELMs): eruptions of the plasma edge lasting $\sim 100\mu\text{s}$ during which time up to 10% of the total plasma stored energy may be lost¹. The role of ELMs in flushing the plasma of impurities may be beneficial, but this is at the cost of potentially damaging localised heat loading on plasma facing components. The increased heat loading generated by ELMs on next generation devices such as ITER necessitates these instabilities either be eliminated entirely or else that their frequency be increased so that the energy released during each ELM is reduced to an acceptable level.

A simplified representation of the ELM cycle is shown in Figure 1 illustrating the ELM cycle as a path through a configuration space characterised by edge pressure gradient and edge current density. Immediately following an ELM, the plasma is stable and resides in the green shaded region. As the plasma heats up, the edge pressure gradient increases. This may then lead to an increase in the edge current density via, for example, the bootstrap mechanism. Departure from the green region leads to instability and the triggering of an ELM crash – either due to excess pressure gradient (exciting a "ballooning" mode) or excess current density (exciting a "peeling" mode). The distance in configuration space travelled

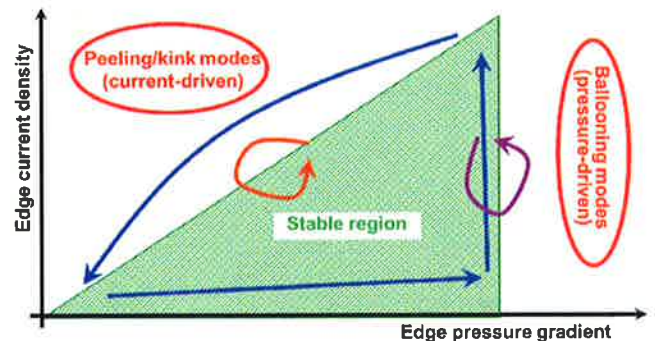


FIG. 1. Simplified diagram of the ELM cycle; small ELMs (represented by the purple and orange arrows) may be operationally acceptable; a large ELM (represented by the blue arrows) may be damaging to plasma facing components. Calculating a realistic stability diagram and then comparing experimentally observed instability thresholds to those predicted by theory is crucial for understanding the physics of ELMs; the problem being addressed by SAMI is that no method currently exists for the routine measurement of the edge current density.

during the crash is related to the stored energy that is released; relatively small cycles (indicated by the orange and purple arrows) may be sufficiently small as to be unproblematic. However, a large crash (indicated by the blue arrows) may lead to damage of plasma-facing components. In order to develop and constrain meaningful models of ELMs, observations of ELMs from experiments are used to locate points on the stability boundary; these observations are then compared with model calculations of the stability boundary. Being able to locate an ELM

event on the stability diagram depends on good diagnostics. The edge pressure gradient can be measured using Thomson scattering^{2,3}. However, there does not currently exist a routine technique for measuring the edge current density – the vertical coordinate on the stability diagram itself has to be calculated from models e.g. by using a neoclassical model to calculate the bootstrap current from the edge pressure gradient. This reliance on a model is unsatisfactory since the model may not capture all the relevant physics. SAMI’s ultimate objective is therefore to make spatially-resolved measurements of the magnetic pitch angle and thence the edge current density.

II. PRINCIPLES OF PHASED-ARRAY IMAGING

Phased-array imaging is an interferometric technique: it uses the phase of the signal at each antenna, rather than focusing optics, to determine the emission pattern. For an extended source, the van Cittert-Zernike theorem tells us that the cross-correlation of signals at the antenna array corresponds to the spatial Fourier transform of the source; the effective aperture is given by the maximum distance between a pair of antennas in the array. Unlike a directly focused system, the resolution is proportional to the square of the number of antennas (since it depends on the number of cross-correlations that can be made between antenna pairs) at the cost of having to capture the phase, as well as the amplitude, of the signal at each antenna.

Aperture synthesis was pioneered as a technique in radio astronomy^{4,5} and is now used widely in that field (see [6] for a comprehensive review). However, to the best of our knowledge, SAMI is the first diagnostic to employ 2-D phased-array imaging in a laboratory plasma diagnostic.

III. 2-D DOPPLER BACK-SCATTERING

The theory of Doppler back-scattering (DBS) is not entirely straightforward; a review of conventional DBS may be found in reference [7] and a detailed description of the extension to 2-D is given in [8]. The technique for measuring magnetic pitch angle relies on the cut-off surface being corrugated, for example as a consequence of turbulence. These corrugations are assumed to be elongated along field lines, since parallel transport is much faster than perpendicular transport. When the plasma is illuminated, the strongest reflected signal comes from the region on the plasma surface normal to the beam. However, this component has only a small Doppler shift and so, assuming the plasma is rotating poloidally and/or toroidally, can be filtered out. The strongest Doppler-shifted signal comes from the regions of the plasma where the density corrugations (and hence magnetic field lines) are perpendicular to the line of sight. The line segment

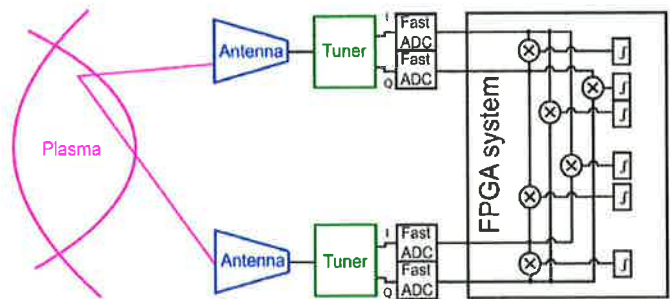


FIG. 2. Simplified diagram of the SAMI hardware. Each of the three sections (i) antenna array (shown in blue) (ii) microwave tuner (shown in green) and (iii) FPGA-based digitisation system (shown in black) are described in the text.

joining the points of strongest blue- and red-shift is therefore expected to be perpendicular to the magnetic field, whence we derive our measurement for the field line pitch. Although not attempted in this Paper, by measuring the field line pitch at more than one frequency (and therefore more than one location, localised by Thomson scattering), using the $1/R$ dependence of the toroidal field in the plasma edge to derive the total field and then applying Ampère’s Law, we can use SAMI to calculate the edge current density.

IV. HARDWARE DESCRIPTION

In this section we provide an overview of the SAMI hardware; a more detailed description is provided in [9]. A simplified diagram of the SAMI hardware is shown in Figure 2. We decided to perform the cross-correlations in software rather than by using mixers. This is beneficial because (i) it permits greater flexibility and control (particularly in terms of calibration) (ii) the number of mixers scales like the square of the number of antennas; but it comes at the cost of more demanding digitisation.

SAMI has 16 independent frequency channels in the range 10-34.5GHz. This frequency range is chosen to cover the steep gradient region in the edge of H-mode plasmas. The cut-offs for O-mode and X-mode for NSTX-U plasmas operating in both L-mode and H-mode are shown for two different times during shot 204672 in Figure 3. The distance between cut-off surfaces corresponding to neighbouring SAMI frequency channels is typically $< 1\text{mm}$; this clearly increases for L-mode. This tight spacing of cut-off surfaces means that, at least in principle, SAMI has excellent spatial resolution.

A. Antenna array

The SAMI antenna array consists of 10 Vivaldi PCB antennas, each measuring $20 \times 60\text{mm}$. These antennas provide good broadband response in the desired range 10-34.5 GHz, a wide field of view (in excess of ± 40 deg in

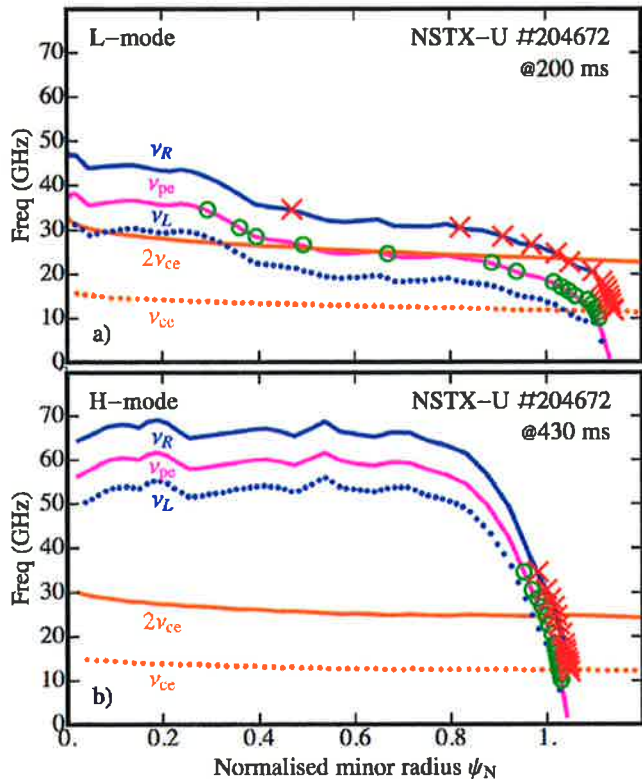


FIG. 3. Diagram showing the electron cyclotron frequency (dashed orange) and its second harmonic (solid orange), the left-hand (dashed blue) and right-hand (solid blue) cut-offs, and the plasma frequency (magenta). The O-mode and X-mode cut-off locations for each of SAMI's 16 frequency channels are shown as green circles and red crosses, respectively. Plots are shown for NSTX-U shot 204672 at two different times namely (a) 200ms and (b) 430ms into the shot, demonstrating how the distribution of SAMI cut-off locations in the plasma changes from L-mode to H-mode. The cut-off spacing between frequency channels in H-mode is typically < 1 mm.

both E and H planes) and excellent polarisation separation. Additionally they are very cheap to manufacture. However, they have the disadvantage that the array is 3-D and so the incoming signal is reflected around inside the array. Eight of the antennas are used as a receiving array; their placement has been chosen to maximise the mean beam efficiency (i.e. to minimise the side-lobe power)¹⁰. The remaining two antennas are used to launch a broad illuminating beam at two user-determined frequencies (typically 10 MHz and 12.5 MHz) above the probing frequency. The back-scattered signal has a bandwidth < 1 MHz and consequently SAMI can image both the spontaneous thermal plasma emission and the back-scattered signal simultaneously.

B. Microwave tuner

The microwave tuner unit operates using the standard heterodyne down-conversion principle. The signal from each receiving antenna is amplified by a low-noise amplifier, split into in-phase and quadrature (I & Q) components by a 90 deg phase-shifter, and frequency down-converted using second harmonic mixers. A reverse process generates the active probing signal on the two transmitting antennas. Connectorised components are used throughout to simplify assembly and reduce design overhead. There are 16 local oscillator sources of dielectric resonance oscillator type approximately evenly spaced (avoiding exact harmonics) in the range 5-17.25 GHz; the choice of source can be switched with a settling time of 100ns.

C. FPGA-based digitisation system

The digitisation requirements are demanding: SAMI acquires data at 250 mega-samples per second and 14 bits per sample (2 aligned bytes), corresponding to a total data rate of 8GB/s continuously over a shot length of 500ms. We designed and built a custom data acquisition unit based on 4DSPs FMC108 ADC card and Xilinx ML605 FPGA board running embedded Linux¹¹. A number of enhancements have been made for SAMI's move from MAST to NSTX-U as described in 12. The standard aperture synthesis image inversion is performed using a CUDA code on an nVidia GPU card¹³ which provides at least an order of magnitude speed-up relative to calculation on a standard CPU. An advantage of phased-array imaging is that, in order to overcome near-field effects, the focal length of the imaging beam can be adjusted in software post-shot (and as a function of viewing direction, if so desired).

V. DEPLOYMENT ON MAST AND NSTX-U

SAMI was originally deployed on the Mega-Amp Spherical Tokamak¹⁴ (MAST) at Culham Centre for Fusion Energy for the period 2011-2013. During this time, SAMI successfully demonstrated the feasibility of 2-D phased-array microwave imaging. In "passive imaging" mode it captured the first 2-D images of O-X-B mode conversion from a tokamak plasma¹⁵ and demonstrated the existence of strong microwave bursts during ELMs (explained via the anomalous Doppler instability)¹⁶. In "active probing" mode, it made the first measurements of edge pitch angle using 2-D Doppler back-scattering⁸, some results from which are presented in this Paper for the first time.

Following the commencement of construction of MAST-Upgrade, SAMI was moved to Princeton Plasma Physics Laboratory where it was installed on the National Spherical Torus Experiment Upgrade¹⁷ (NSTX-U)

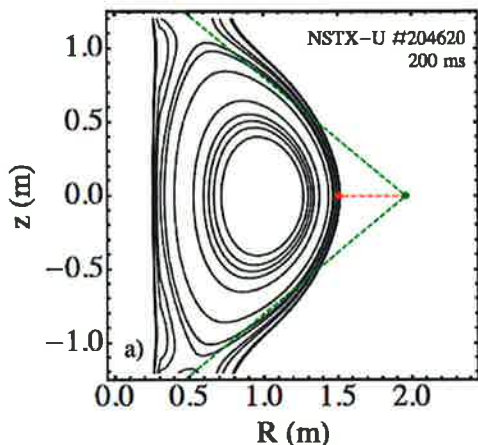


FIG. 4. Diagram showing installation position of the SAMI antenna array on NSTX-U and the critical density flux surfaces for SAMI's frequency channels for NSTX-U shot 204620 at 200ms (derived from the midplane Thomson scattering data and approximating density to be a flux function). SAMI's field of view is shown in green; the normal viewing ray is shown in red.

with only minor modifications to the hardware. SAMI began collecting data on May 3rd, 2016. The first data from SAMI on NSTX-U is presented in this Paper.

As shown in Figure 4, the SAMI antenna array is installed on NSTX-U at the outboard midplane. SAMI has a good view of the plasma (extent shown in green in the Figure). The nearest point on the plasma last closed flux surface (ray shown in red in the Figure) is approximately 0.5m from the array. We have illustrated the critical density flux surfaces corresponding to each of SAMI's frequency channels by using the midplane Thomson scattering data and approximating density to be a flux function. On MAST, SAMI was located approximately 1m away from the plasma LCFS and 20cm above the midplane; the view was partially obscured by one of the poloidal field coils. The location on NSTX-U is an improvement since there are no vessel components obscuring the view, the proximity to the plasma increases the amplitude of the back-scattered signal (see below) and the location on the midplane will enable future studies testing theories of polarisation-dependent asymmetries in OXB mode conversion in double null discharges. However, the distance between the antennas and the plasma is now only approximately three times the largest distance between antenna pairs, which means that we are approaching the near field. This may necessitate some further development of our image inversion algorithms.

VI. RESULTS

Typical Doppler-shifted spectra from an individual SAMI antenna from both MAST and NSTX-U are shown

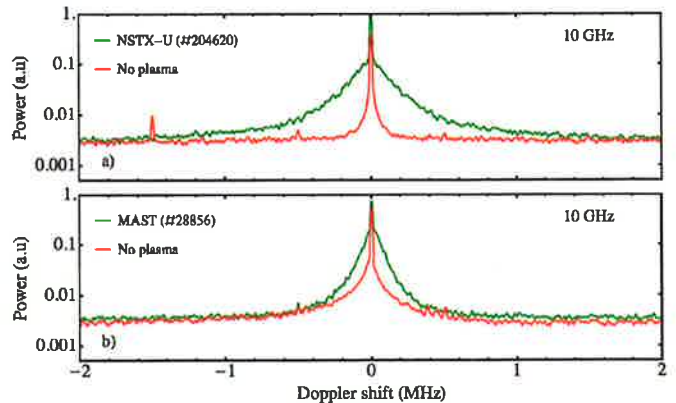


FIG. 5. Plot of the active probing spectrum on both MAST and NSTX-U shown with no plasma (red) and during a discharge (green) for SAMI's lowest frequency channel (10GHz). The increase in signal is greater in NSTX-U than in MAST due to SAMI's antenna array being closer to the plasma surface in NSTX-U.

in Figure 5. The spectra shown in red are measured before the start of the shot i.e. when no plasma is present. As expected, the reflected signal has relatively narrow bandwidth (since the surfaces from which the beam is reflecting are stationary). The spectra shown in green are measured during a shot i.e. when plasma is present. As expected, there is a significant increase in the Doppler-shifted power. Moreover, we observe that the Doppler-shifted power on NSTX-U is significantly greater than the Doppler-shifted power on MAST due to the antenna array being closer to the plasma surface on NSTX-U. Unlike conventional "single ray" Doppler back-scattering, the signal comes not from a small region of the plasma but from an extended area. Consequently the Doppler spectrum that SAMI sees is not a well-defined spike (at a frequency proportional to the plasma velocity) but rather a smeared-out spectrum. Steering the beam using all eight antennas leads to an imbalance between the red-shifted and blue-shifted power as a function of viewing direction, but it is not currently possible to extract a rotation speed from these data.

Figure 6 shows data from MAST shot 27894 and compares the SAMI magnetic pitch angle measurement (shown in green) with unconstrained EFIT (shown in red) and the motional Stark effect (MSE) measurement (shown in purple). This measurement is made at 16GHz, corresponding to a density surface that is just outside the last closed flux surface (as shown in panel (c)). A reasonable level of agreement between SAMI, MSE and EFIT in the measured pitch angle is observed up to 240ms. At around 240ms, the discharge transitions from L-mode to H-mode (as can be seen in the D_α spectrum shown in panel (g)). During this later period (as shown in panel (b)), the Doppler-shifted power reduces so much that a SAMI reconstruction becomes impossible. This is due to the reduction in the amplitude of edge turbulence associated with H-mode. This problem could be overcome by

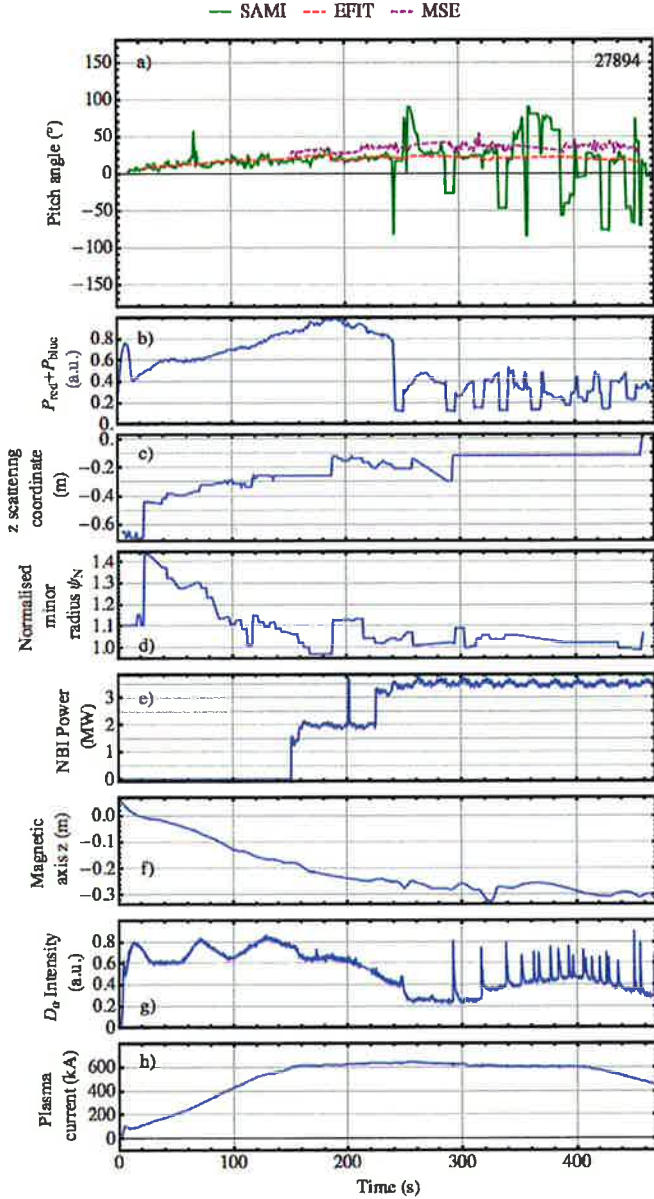


FIG. 6. Data from MAST shot 27894 operating in L-mode before 240ms and H-mode thereafter. Panel (a) compares the SAMI measurement of the edge pitch angle at 16GHz with MSE and EFIT. The other panels provide contextual information for this shot.

increasing the power in the probing beam.

Figure 7 shows data from NSTX-U shot 204620 and compares the SAMI magnetic pitch angle measurement (shown in green) with unconstrained EFIT (shown in red). (MSE data is not available for this shot.) This measurement is made at 10GHz, corresponding to a density surface significantly outside the last closed flux surface. The SAMI measurement follows the EFIT calculation but is larger by a factor of 2. It appears that the plasma enters H-mode at approximately 250ms. At this time, the SAMI Doppler-shifted power experiences a re-

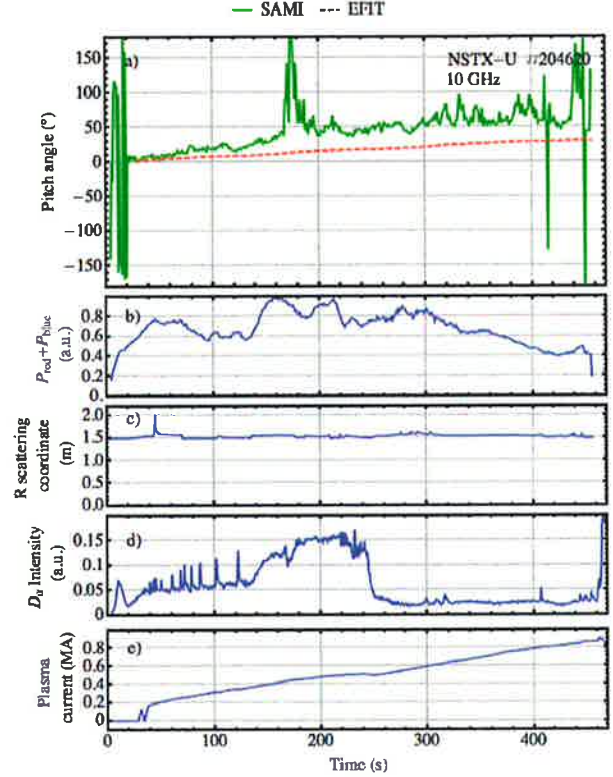


FIG. 7. Data from NSTX-U shot 204620 operating in L-mode before 250ms and H-mode thereafter. Panel (a) compares the SAMI measurement of the edge pitch angle at 10GHz with MSE and EFIT. The other panels provide contextual information for this shot.

duction, but not to the same extent as seen on MAST, thereby enabling SAMI to continue working.

VII. SUMMARY AND FUTURE WORK

In this Paper we have motivated SAMI in terms of needing a direct measurement of the edge current density in order to develop and constrain models for ELMs. Having briefly described the principles of phased-array imaging and the SAMI hardware, we presented new results comparing the edge pitch angle measured by SAMI with EFIT and MSE on MAST and with EFIT on NSTX-U. There appears to be a good agreement between the three independent MAST measurements. The SAMI measurement on NSTX-U is consistently a factor of two larger than the EFIT calculation throughout the measurement window; this discrepancy is currently unexplained, but may be related to the cut-off surface being so far outside the last closed flux surface. In summary we claim that SAMI has demonstrated the feasibility of measuring the edge pitch angle via 2-D Doppler back-scattering.

Moving this methodology from proof-of-principle to production quality requires a number of technical upgrades that we look forward to implementing in the near

future: (a) the separation of polarisations to reduce interference between O-mode and X-mode reflections (b) an increase in the number of antennas to reduce the side-lobe power to a level comparable to a focused system (c) acquisition of two frequencies simultaneously so that time-resolved measurements of the magnetic shear (and thence current density) can be obtained.

ACKNOWLEDGEMENTS

This work was funded, in part, by the University of York, the UK EPSRC under grants EP/H016732 and EP/K504178, the RCUK Energy Programme under grant EP/I501045 and by the US DoE under contract DE-AC02-09CH11466. This work has been carried out within the framework of the EUROfusion Consortium and has received funding from the Euratom research and training programme 20142018 under Eurofusion project ER-WP15_CCFE-03. The views and opinions expressed herein do not necessarily reflect those of the European Commission.

¹H. Zohm, *Plasma Physics and Controlled Fusion* **38**, 105 (1996).

²R. Scannell, M. Walsh, M. Dunstan, J. Figueiredo, G. Naylor, T. OGorman, S. Shibaev, K. Gibson, and H. Wilson, *Review of Scientific Instruments* **81**, 10D520 (2010).

³B. LeBlanc, A. Diallo, G. Labik, and D. Stevens, *Review of Scientific Instruments* **83**, 10D527 (2012).

⁴M. Ryle and A. Hewish, *Monthly Notices of the Royal Astronomical Society* **120**, 220 (1960).

⁵M. Ryle, *Nature* **239**, 435 (1972).

⁶A. R. Thompson, J. M. Moran, and G. W. Swenson Jr, *Interferometry and synthesis in radio astronomy* (John Wiley & Sons, 2008).

⁷E. Holzauer, M. Hirsch, T. Grossmann, B. Braas, and F. Serra, *Plasma Physics and Controlled Fusion* **40**, 1869 (1998).

⁸D. Thomas, K. Brunner, S. Freethy, B. Huang, V. Shevchenko, and R. Vann, *Nuclear Fusion* **56**, 026013 (2016).

⁹V. F. Shevchenko, R. G. Vann, S. J. Freethy, and B. K. Huang, *Journal of Instrumentation* **7**, P10016 (2012).

¹⁰S. Freethy, V. Shevchenko, and R. Vann, *Antennas and Propagation, IEEE Transactions on* **60**, 5442 (2012).

¹¹B. Huang, R. Vann, S. Freethy, R. Myers, G. Naylor, R. Sharples, and V. Shevchenko, *Fusion Engineering and Design* **87**, 2106 (2012).

¹²K. Brunner, J. Chorley, N. Dipper, G. Naylor, R. Sharples, G. Taylor, D. Thomas, and R. Vann, *Review of Scientific Instruments* (2016), (submitted to the proceedings of this conference).

¹³J. Chorley, R. Akers, K. Brunner, N. Dipper, S. J. Freethy, R. Sharples, V. Shevchenko, D. A. Thomas, and R. G. Vann, *Fusion Science and Technology* **69** (2016).

¹⁴I. Chapman *et al.*, *Nuclear Fusion* **55**, 104008 (2015).

¹⁵S. Freethy, B. Huang, V. Shevchenko, and R. Vann, *Plasma Physics and Controlled Fusion* **55**, 124010 (2013).

¹⁶S. Freethy, K. McClements, S. C. Chapman, R. Dendy, W. Lai, S. Pamela, V. F. Shevchenko, and R. Vann, *Physical Review Letters* **114**, 125004 (2015).

¹⁷J. Menard *et al.*, *Nuclear Fusion* **52**, 083015 (2012).

Princeton Plasma Physics Laboratory Office of Reports and Publications

Managed by
Princeton University

under contract with the
U.S. Department of Energy
(DE-AC02-09CH11466)

P.O. Box 451, Princeton, NJ 08543
Phone: 609-243-2245
Fax: 609-243-2751

E-mail: publications@pppl.gov

Website: <http://www.pppl.gov>